6(2009) 229 – 245



Latin American Journal of Solids and Structures
www.lajss.org

Dynamic fracture analysis of concrete or rock plates by means of the Discrete Element Method

Abstract

The authors apply the so-called Discrete Element Method (DEM) to determine the dynamic response of concrete and rock plates of various sizes that fracture under the action of static and dynamic loading. When, on account of the size of the model, larger elements must be employed, the issue of mesh objectivity must be addressed. In response determinations of structures with initial cracks or high stress gradients, which result in fracture localization, well established procedures lead to results that appear to be mesh independent. However, in elements subjected to approximately uniform stress fields a hitherto unknown problem arises in the analysis of non-homogeneous materials: the need to know *a priori* the degree of fracturing of the element. This should also affect finite element analysis in cases in which there is no clear fracture localization. In order to provide additional evidence on fracture localization, plates of different sizes subjected to external uni-axial tensile loading under different levels of stress localization are investigated in this paper. The effective stress-strain relationship, ultimate tensile stress and strain, dissipated fracture energy and fracture patterns are determined for plates ranging in size from 0.25 to 15m. Difficulties associated to the prediction of the behavior of large nonlinear structural systems are discussed in connection with the available results.

Keywords

fracture analysis, Discrete Element Method, mesh independence, size effect.

Ignacio Iturrioz[a,*], **Letícia Fleck Fadel Miguel**[b] **and Jorge Daniel Riera**[c]

[a]Department of Mechanical Engineering, Federal University of Rio Grande do Sul, Porto Alegre, RS – Brazil.
[b]Department of Mechanical Engineering, Federal University of Rio Grande do Sul, Porto Alegre, RS – Brazil.
[c]Department of Civil Engineering, Federal University of Rio Grande do Sul, Porto Alegre, RS – Brazil.

Received 3 May 2009;
In revised form 6 Aug 2009

* Author email: ignacio@mecanica.ufrgs.br

1 INTRODUCTION

The determination of the static or dynamic response of solids by means of numerical methods, such as Finite Differences (FDM), Finite Elements (FEM) or Discrete Elements (DEM) requires the estimation of computational errors, *i.e.*, the sensitivity of the solutions to the size or other features of the mesh adopted in the analysis. In Linear Elasticity problems the issue is commonly addressed by comparing solutions obtained with increasingly finer meshes

until convergence is reached with the desired accuracy. In Linear Elastic Fracture Mechanics (LEFM), a similar approach is possibly the only feasible alternative to assess convergence of the solution. The performance of the DEM has been evaluated both in the solution of Linear Elasticity problems as well as in connection with problems of LEFM, as a preliminary step before applying the method to non-linear problems (Iturrioz, [4]; Dalguer *et al.*, [2]; Miguel *et al.*, [8]).

Figure 1 shows the critical stress in a homogeneous plate with an edge crack subjected to a uniform tensile stress applied at the upper and lower plate boundaries according to theoretical LEFM and computed using a DEM model by Rocha and Riera [17]. The length of the elements was in all cases equal to 0.01m, size that appears to yield accurate results except in the case of the shortest edge crack, which might require adopting a finer mesh. In such cases, assessing the adequacy of a given mesh presents no difficulty except eventually high computational costs.

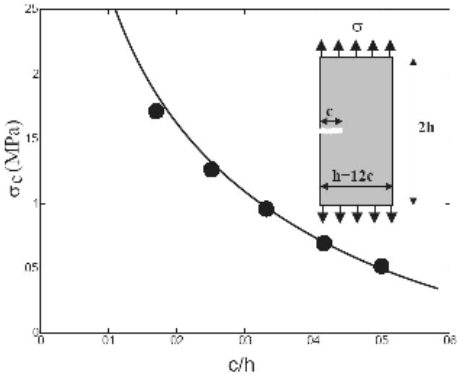

Figure 1 Critical stress for tensile fracture of a rectangular plate (0.12×0.24m) in plane stress with edge crack computed by DEM model (solid dots) and predicted by LEFM (Rocha and Riera, [17]).

A somewhat different situation appears in the solution of problems involving non-homogeneous materials, because in such case the size of the elements must be sufficiently small both in relation to the size of the crack as well as in relation to the correlation lengths of the fields that model the material non-homogeneities (Riera *et al.*, [13]). These requirements can rarely be met in engineering practice on account of the resulting computational costs, demanding resort to larger DEM or FEM elements. In this context, the static strength of rock dowels was numerically determined by Miguel *et al.* [8]. In this case a cubic rock dowel fixed at its base is subjected to a uniform tangential stress (shear) at its upper face, which results in strong fracture localization. In such case renders the effect investigated in this paper is marginal.

In fact the DEM, as employed by the authors for determining the response of homogeneous solids subjected to arbitrary static or dynamic loading, including LEFM problems, is robust and reliable. In case of non-homogeneous materials, the authors obtained solutions by simulation, generating samples of the random fields that define the spatial variation of material properties (Rios and Riera, [15]; Miguel *et al.*, [8]). In such case, the issue of fracture localization requires a more detailed examination, which is the subject of this paper. The basic features of the DEM in these applications are summarized in Section 2. Examples that cover the full response of

plates subjected to tension are then presented in Section 3, providing numerical evidence for the evolution of fracture localization with size.

2 THE DISCRETE ELEMENT METHOD IN FRACTURE PROBLEMS

The Discrete Element Method employed in this paper is based on the representation of a solid by means of an arrangement of elements able to carry only axial loads. The equivalence between an orthotropic elastic continuum and the cubic arrangement of uni-axial elements consisting of a cubic cell with eight nodes at its corners plus a central node was shown by Nayfeh and Hefzy [9]. The discrete elements representation of the orthotropic continuum was adopted by the authors to solve structural dynamics problems by means of explicit direct numerical integration of the equations of motion, assuming the mass lumped at the nodes. Each node has three degrees of freedom, corresponding to the nodal displacements in the three orthogonal coordinate directions.

The equivalence between the orthotropic elastic solid with the principal material axes oriented in the direction parallel to the longitudinal elements of the discrete elements model was extensively verified by Hayashi [3]. The equations that relate the properties of the elements with the elastic constants of an isotropic medium are:

$$\delta = \frac{9\nu}{4-8\nu}, E_A = EA_n = EL_0^2\frac{(9+8\delta)}{2\,(9+12\delta)}, EA_d = \frac{2\sqrt{3}}{3}A_n \tag{1}$$

in which E and ν denote Young's modulus and Poisson's ratio, respectively, while An and Ad represent the areas of normal and diagonal elements.

The resulting equations of motion may be written in the well-known form:

$$M\ddot{\vec{x}} + C\dot{\vec{x}} + \vec{F}_r\,(t) - \vec{P}\,(t) = 0 \tag{2}$$

in which $\vec{x}$ represents the vector of generalized nodal displacements, $\boldsymbol{M}$ the diagonal mass matrix, $\boldsymbol{C}$ the damping matrix, also assumed diagonal, $\vec{F}_r\,(t)$ the vector of internal forces acting on the nodal masses and $\vec{P}\,(t)$ the vector of external forces. Obviously, if $\boldsymbol{M}$ and $\boldsymbol{C}$ are diagonal, Equations (2) are not coupled. Then the explicit central finite differences scheme may be used to integrate Equation (2) in the time domain. Note that the location of each nodal mass is defined by three coordinates, rotational degrees of freedom being disregarded. Since the nodal coordinates are updated at every time step, large displacements can be accounted for in a natural and efficient manner.

Thus, in all cases the integration is performed employing the explicit central finite differences method. Therefore, the integration time step must to be smaller than a critical value $\Delta tcrit$, which may be estimated as $0.6L_0\Big/\sqrt{E/\rho}$, in which the denominator represents the velocity of propagation of P-waves in an isotropic elastic medium. The numerator denotes the length of the shortest elements in the model, *i.e.*, the diagonal bars.

In the present paper, the relation between tensile stress and strain in the material was assumed to be triangular, as indicated in Figure 2. The limit strain ϵr is determined to satisfy

the condition that, upon rupture of the element, once the strain reaches the value ϵr, energy *Uelem* is liberated, according to Equation (3):

$$U_{elem} = \frac{A_f G_f}{L_0} \tag{3}$$

in which *Af* is the fractured area bar, *L0* is the normal bar length and *Gf* is the specific fracture energy that characterized the material toughness.

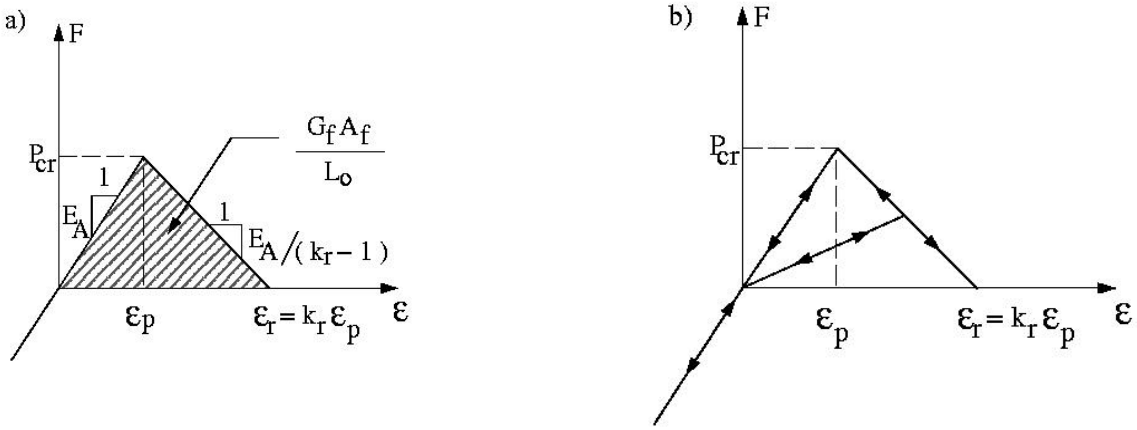

Figure 2 Triangular constitutive law for brittle material.

Note that the fracture energy, *i.e.*, the energy dissipated by the total rupture of one element, depends on the numerator of Equation (3), which is the product of the fracture area within the element under consideration, times the specific fracture energy of the material. In previous papers (Rocha, [16]; Riera and Iturrioz, [10]; Miguel *et al.*, [8]), the assumption that *Af equals the area of the basic brick element* L_0^2 was implicit. On that basis, the fracture area of the longitudinal bars is given by:

$$A_f = c_a L_0^2 \tag{4}$$

in which the coefficient *ca* was computed as 0.1385. For diagonal bars, *ca* equals 0.1593. This assumption is valid as long as there is a strong localization effect, leading to a rupture configuration characterized by a single large crack. For example, fracture of rock dowels analyzed by Miguel *et al.* [8] occurs in most cases as a single crack that, starting near the intersection between the dowel wall and the foundation, propagates through the dowel, as illustrated in Figure 3. As more cracks extend throughout the volume of the element, the coefficient *ca* should increase, since the fractured area is larger.

Another important feature of the model is the assumption that all material properties, such as *E*, ρ and *Gf*, may be described by random fields, *i.e.* they can vary randomly throughout the structure. In this paper, a Weibull probability distribution was adopted for the specific fracture energy. It should be underlined again that fracture localization weakens as the non-homogeneous nature of the material becomes more pronounced, *i.e.*, as the coefficients of

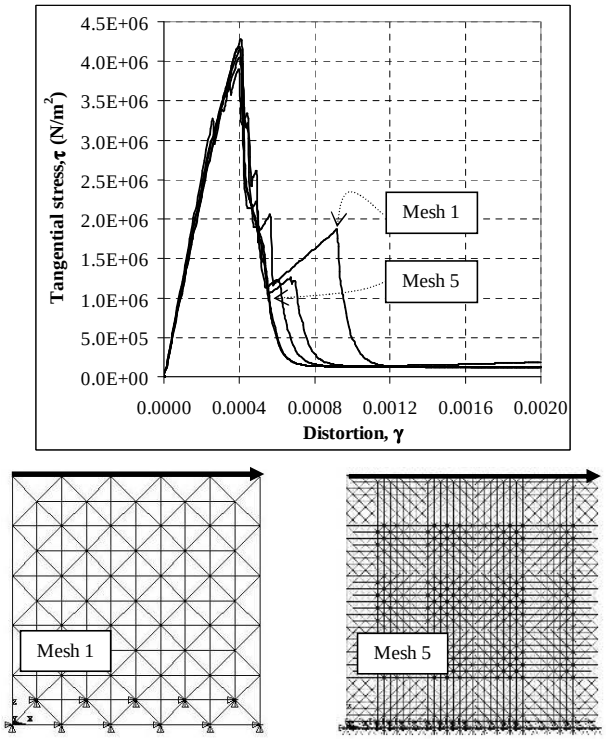

Figure 3 (a) Tangential stress *vs.* distortion for a 1m cube computed using five different meshes. (b) Mesh 1: 5×5×5 cubic modules, (c) Mesh 5: 20×20×20. In all cases a large crack that follows closely the lower edge occurs, with minor damage elsewhere.

variation of the fields that describe the material properties increase. On account of this effect, LEFM solutions for plates with edge cracks, such as the theoretical and numerical values shown in Figure 1, for example, may not be valid in case of non-homogeneous materials like concrete or rock.

Applications of the DEM in studies involving non-homogeneous materials subjected to fracture, like concrete and rock, may be found in Iturrioz [4], Riera and Iturrioz [10], Dalguer *et al.* [1], Rios [14] and Miguel *et al.* [8]. Additionally, Dalguer *et al.* [2], Riera *et al.* [12], Miguel [5], Miguel *et al.* [7] and Miguel and Riera [6], also applied the method to solve problems involving rupture of concrete or rock.

3 SIZE EFFECT IN FRACTURE ANALYSIS OF NON-HOMOGENEOUS PLATES

3.1 Concrete plates

Concrete plates under a plane strain condition, fixed at the lower face and subjected to tensile stress on the upper face were analyzed up to failure through numerical simulation. The size of the plates ranges from 0.25m to 10.0m. A rectangular plate (Case A) and a rectangular plate with an indentation on both sides (Case B) were simulated. Plate dimensions and DEM mesh

employed in the analysis are indicated in Table 1 (See also Figure 6). The material properties of the concrete are given in Table 2. The coefficients of variation of Gf indicated in Tables 2 and 5 correspond to the individual bar elements, *which are approximately two and a half times larger than the corresponding value for a cubic cell of the same size.*

Table 1 Basic dimensions of the concrete plate samples ($L0 = 0.05m$).

Plate	$\boldsymbol{L}$
Plate 0.25 (5×5)	0.25m
Plate 1.25 (25×25)	1.25m
Plate 6.25 (125×125)	6.25m
Plate 10.0 (200×200)	10.0m

Table 2 Properties of brittle materials: Concrete.

Property	**Value**
E (Young's modulus)	3.5E10N/m^2
ρ (mass density)	2400kg/m^3
ν (Poisson's ratio)	0.25
E(Gf) (expected value of specific fracture energy)	100N/m
ϵp (critical strain)	6.35E-5
CV(Gf) (coefficient of variation of Gf)	40%

Nodal points on the upper face of the specimens were subjected to a controlled uniform displacement that increases smoothly in time, simulating a slowly increasing applied load. Uniform displacements along the upper edge induce a nominally uniform tension in the specimen.

Ten simulations were performed for each case and each plate size. The resulting stress-strain curves for plate size of 0.25m and for size 10m are shown in Figures 4 (a, b, c, and d) for all simulations. Note that the fracture energy is regarded as a 3D random field with the properties indicated in Table 2 and Weibull (Extreme Value Type III, minimum) probability distribution functions, so each virtual test leads to a different strength and a different stress-strain curve. The mean curve for all simulations is also shown in Figures 4, while the mean curves for all sizes in both cases are shown in Figures 5a and 5b.

Typical crack patterns are shown in Figure 6. Undamaged, damaged and totally broken elements are represented in cyan, orange and red, respectively. The models show both a perceptible size effect as well as typical cracking patterns, which quantify the damage distribution in the plates. Table 3 presents the average tensile strength and ultimate strain of the plates, which tend to decrease as the size of the plate increases.

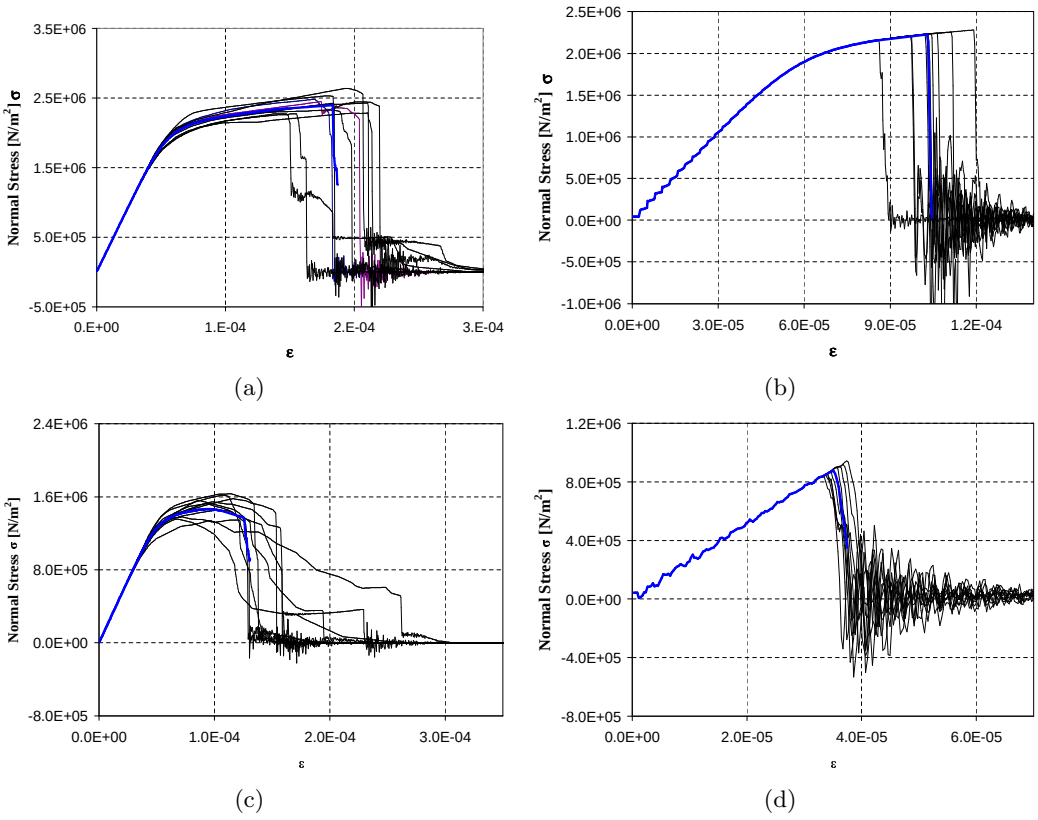

Figure 4 Mean normal stress on the lower face *vs.* mean strain for all simulations and resulting mean curve for all simulations (thick blue line). (a) L = 0.25m (Case A), (b) L = 10.0m (Case A), (c) L = 0.25m (Case B), (d) L = 10.0m (Case B).

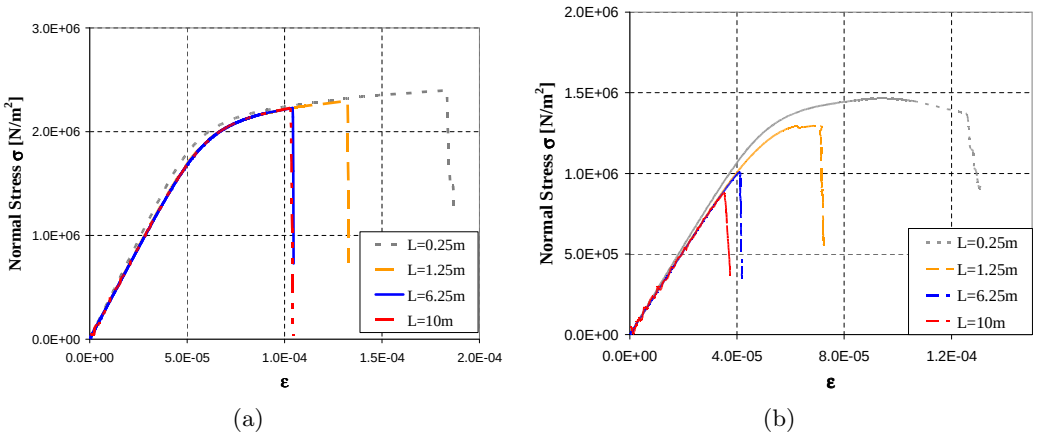

Figure 5 Mean normal stress on the lower face *vs.* mean strain: average curves for all sizes. (a) Case A, (b) Case B.

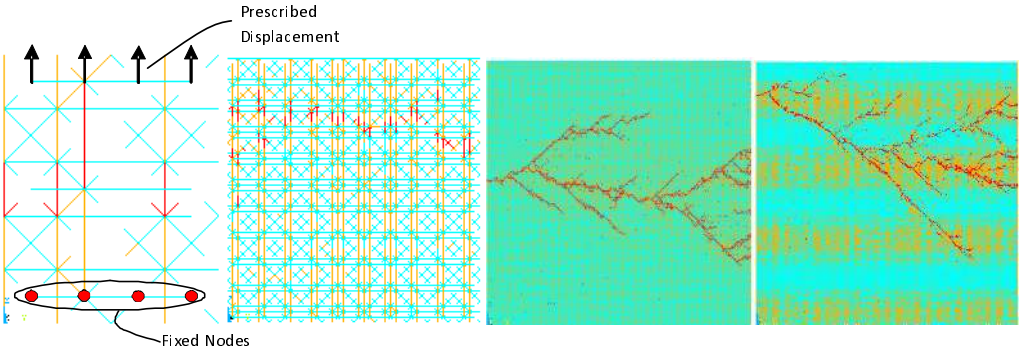

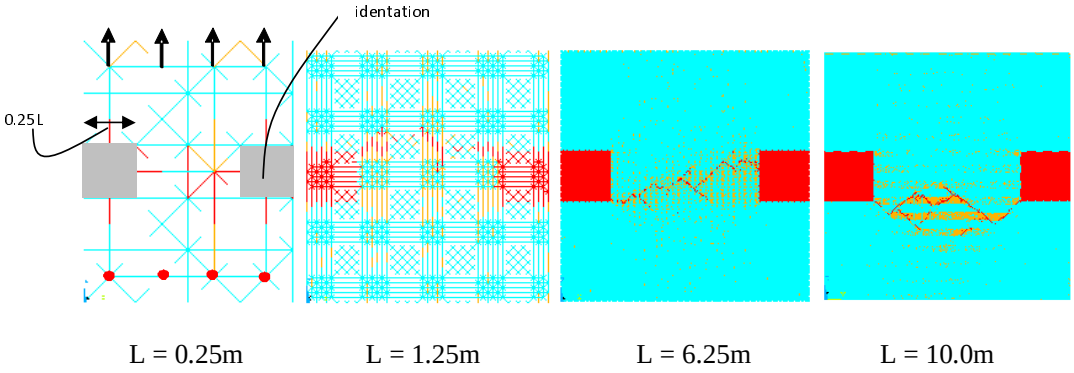

Figure 6 Rupture configuration of concrete plates subjected to uniform tensile stress for all sizes: Upper row Case A, Bottom row Case B.

Table 3 Maximum (rupture) mean tensile stress and strain of simulated concrete plates.

Plate	**Stress σr**	**Strain ϵr**
Plate 0.25	2.41MPa	1.80E-4
Plate 1.25	2.30MPa	1.33E-4
Plate 6.25	2.23MPa	1.06E-5
Plate 10.0	2.23MPa	1.03E-5

3.2 Rock plates

Rock plates under plane stress, fixed at their lower face and subjected to tension on their upper face were analyzed up to failure through numerical simulation. The size of the samples ranges from 1.0 to 15.0m. The response of the specimens may be determined in a similar manner, starting from the constitutive criteria for the individual elements. The smallest array that leads to satisfactory results consists of 10×10×1 cubic modules, with 1026 DOF, used for the 1.0m plate, while the 15.0m plate presents 150×150×1 cubic modules, with 204306 DOF, constituting

the largest array used in this study. Table 4 shows the basic dimensions of the four samples analyzed, while relevant material properties are listed in Table 5.

Table 4 Basic dimensions of the rock plate samples ($L0 = 0.10m$).

Plate	$\boldsymbol{L}$
Plate 1.0 (10×10)	1.0m
Plate 4.0 (40×40)	4.0m
Plate 8.0 (80×80)	8.0m
Plate 15.0 (150×150)	15.0m

Table 5 Properties of brittle materials: Granite rock.

Property	**Value**
E (Young's modulus)	7.5E10N/m^2
ρ (mass density)	2700kg/m^3
ν (Poisson's ratio)	0.25
E(Gf) (expected value of specific fracture energy)	1300N/m
ϵp (critical strain)	1.054E-4
CV(Gf) (coefficient of variation of Gf)	40%

The nodes on the upper face of the specimens were subjected to controlled displacements that smoothly increase from zero to a limit value. In loading case A, uniform displacements along the upper edge induce a nominally uniform tension in the specimen. In loading case B, the test specimens were subjected to a triangularly distributed controlled displacement, inducing a non-uniform tension in the specimen.

Six simulations were carried out for each loading case and for each plate size. For illustration purposes, the resulting stress-strain curves for all simulations for the 4.0m plate are shown in Figure 7, for loading case A. Note that the fracture energy is also considered a random field with the properties indicated in Table 5, so each simulation leads to a different strength and a different stress-strain curve. The probability distribution of Gf was assumed Weibull. The mean curve for all simulations is also shown in Figure 7. The mean curves for all tested sizes are shown in Figure 8.

Next, the plates were subjected to triangularly distributed displacements on their upper face (loading Case B). Six simulations were also performed for each plate size. The resulting stress-strain curves for all simulations for the 4.0m plate are shown in Figure 9, which also presents the mean curve. Figure 10 shows the mean curves for all simulated sample sizes.

Typical cracked granite plates for loading Case A are shown in Figure 11, while Figure 12 presents the cracking patterns for Case B. Again, colors cyan, orange and red represent undamaged, damaged and totally broken (failed) elements, respectively.

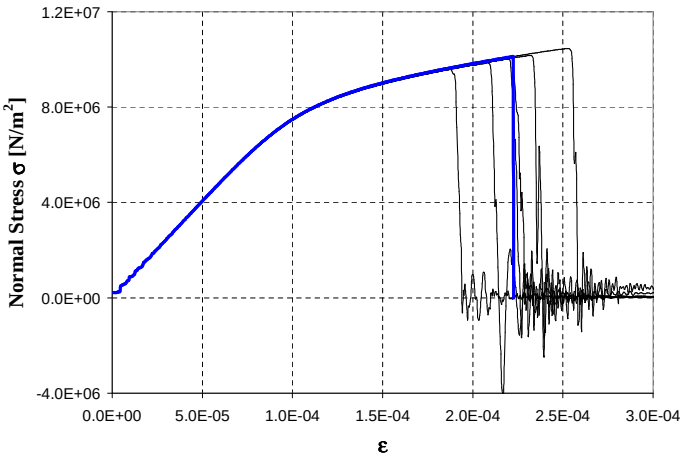

Figure 7 Mean normal stress on the lower face *vs.* mean strain for the 4m plate, for all simulations and resulting average curve (thick blue curve) (Rock Case A – uniform imposed displacements).

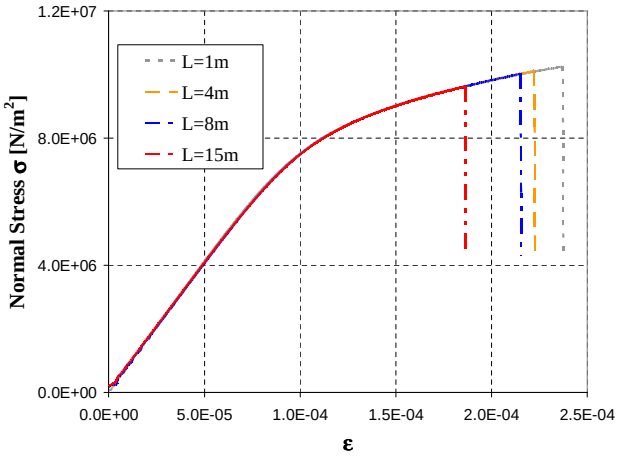

Figure 8 Normal stress on the lower face *vs.* mean strain for the mean curve of all tested sizes (Rock Case A – uniform imposed displacements).

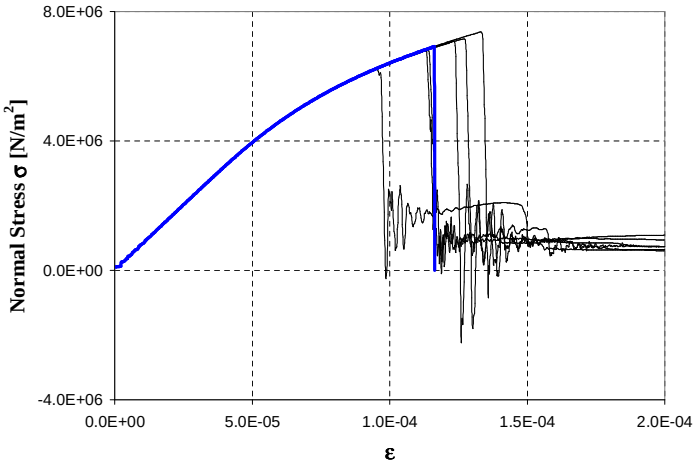

Figure 9 Mean normal stress on the lower face *vs.* mean strain for the 4m plate, for all simulations and resulting average curve, shown by thick blue line (Rock Case B – triangular imposed displacements).

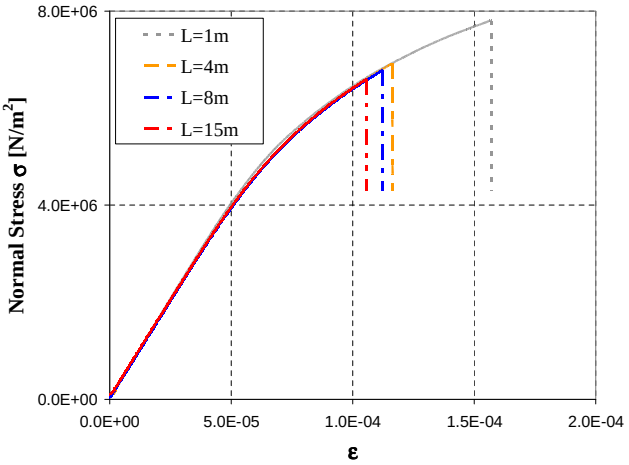

Figure 10 Mean normal stress on the lower face *vs.* mean strain for the mean curve of all tested sizes (Rock Case B – triangular imposed displacements).

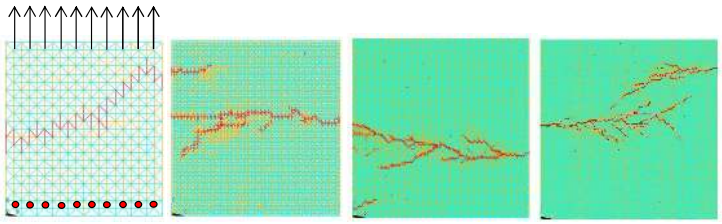

Figure 11 Rupture configuration of rock plates subjected to uniform tensile stress (Case A).

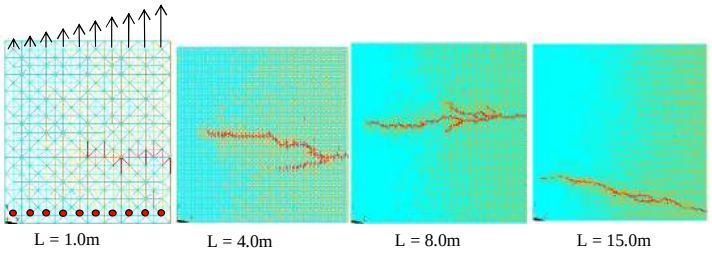

Figure 12 Rupture configuration of rock plates subjected to triangular tensile stress (Case B).

Once again, the models show both a perceptible size effect as well as credible cracking patterns, defining the predicted damage distribution in the plates. The size effect may be detected in Table 6, which illustrates the decrease of the average tensile strength as the size of the plate increases. Damage localization, shown in Figures 11 and 12, is more pronounced in presence of a stress gradient (Case B). Damage, indicated by the orange-tainted regions, as well as crack surfaces, are more widely distributed in loading case A (Figure 11). No experimental results for this size range are known to the authors. At any rate, as discussed below, both features of the non-linear problem should be taken into consideration when large DEM or FEM elements are employed.

Table 6 Maximum (rupture) mean tensile stress and strain of simulated rock plates.

Plate	**Case A**		**Case B**	
	Stress σ_r	**Strain ϵ_r**	**Stress σ_r**	**Strain ϵ_r**
Plate 1.0	10.02MPa	2.38E-4	7.80MPa	1.56E-4
Plate 4.0	10.02MPa	2.28E-4	7.08MPa	1.23E-4
Plate 8.0	10.00MPa	2.18E-4	6.78MPa	1.17E-4
Plate 15.0	9.62MPa	1.91E-4	6.68MPa	1.03E-4

4 INFLUENCE OF SIZE ON APPARENT MATERIAL PROPERTIES

Figure 13(a) shows the normalized coefficients of variation of the ultimate stress and ultimate strain determined in the simulation analysis of concrete plates Case A. The dots represent the CV obtained in ten simulations of each plate size and they are thus affected by statistical error. Nevertheless, a trend towards smaller values of the CV as the size increases is visible. Similar results for the expected values of the maximum stress and strain in terms of the plate size, normalized with respect to the corresponding value for the smallest plate (0.25m), are shown in Figure 13(b). Since the variability of estimates of the mean is smaller than those of the variance, in the former case the dots are closer to a smooth curve. The ultimate strain is clearly more sensitive to size variations than the ultimate stress. Figures 14, 15 and 16 show the results for the others simulated cases.

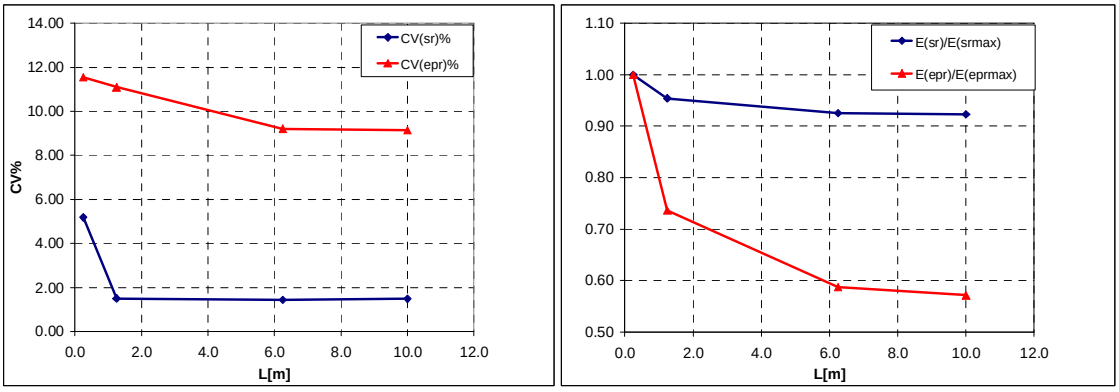

Figure 13 Influence of size in simulations of concrete plates (Case A) under tensile stresses. (a) Variation of CV(σr) and CV(εpr) with plate size, (b) Variation of the mean normalized maximum tensile stress and strain with size.

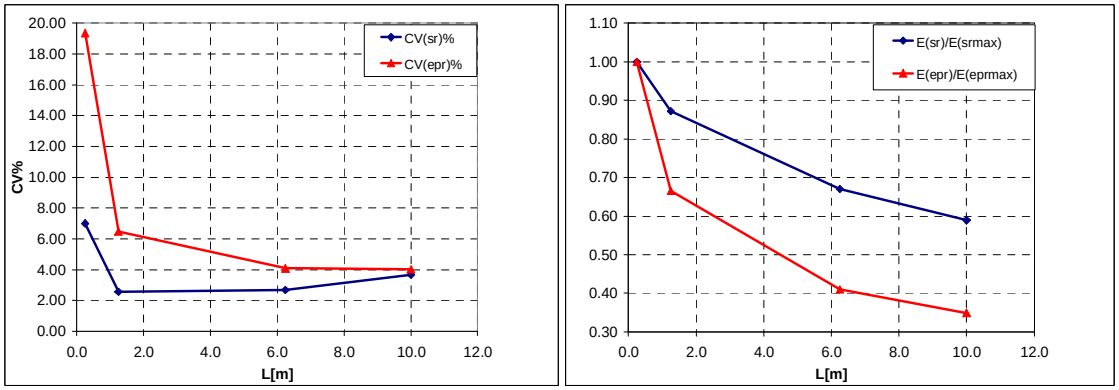

Figure 14 Influence of size in simulations of concrete plates (Case B) under tensile stresses. (a) Variation of CV(σr) and CV(εpr) with plate size, (b) Variation of the mean normalized maximum tensile stress and strain with size.

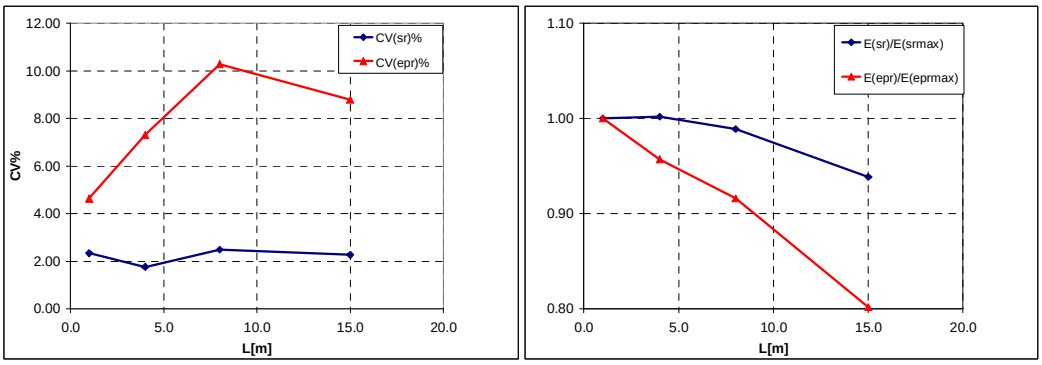

Figure 15 Influence of size in simulations of rock plates under tension (Case A). (a) Variation of CV(σr) and CV(εpr) with plate size, (b) Variation of the mean normalized maximum tensile stress and strain with size.

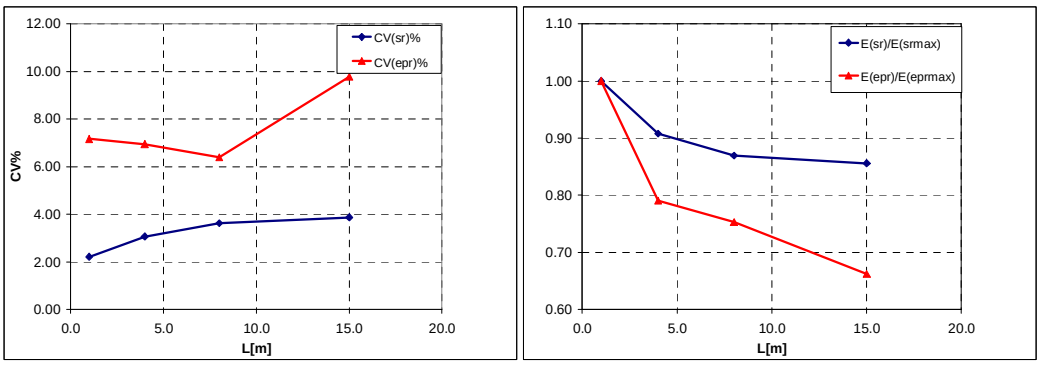

Figure 16 Influence of size in simulations of rock plates under tensile stresses (Case B). (a) Variation of CV(σr) and CV(εpr) with plate size, (b) Variation of the mean normalized maximum tensile stress and strain with size.

The normalized mean strain for various sizes estimated by simulation, for both concrete and rock plates is shown in Figure 17(a), while Figure 17(b) shows the normalized mean maximum tensile strength for both concrete and rock plates for various sizes. Figure 17 also shows experimental results obtained by Van Vliet and Van Mier [18] in concrete and sandstone samples. A more pronounced size effect in the experimental results than in the numerical simulations is perceptible (in Case A for concrete and in Cases A and B for rock plates). This fact is explained by observing that the experimental samples have the shape of an eight, that is, a neck that tends to induce the localization of rupture at the section with smallest area.

Figures 18(a) and 18(b) show the CV of the ultimate strain and ultimate stress, respectively, for both concrete and rock plates. In the presence of strong localization (rock plate, Case B), the last figures show a perceptible trend to larger variances as the size of the specimens increases, not only for the rupture strain εpr but also for the maximum stress σr. This trend may be due to the fact that when localization occurs the material properties linked with the strength such as Gf or σmax over a small region of the specimen are responsible for the definition of the rupture parameters previously defined (εpr , σr).

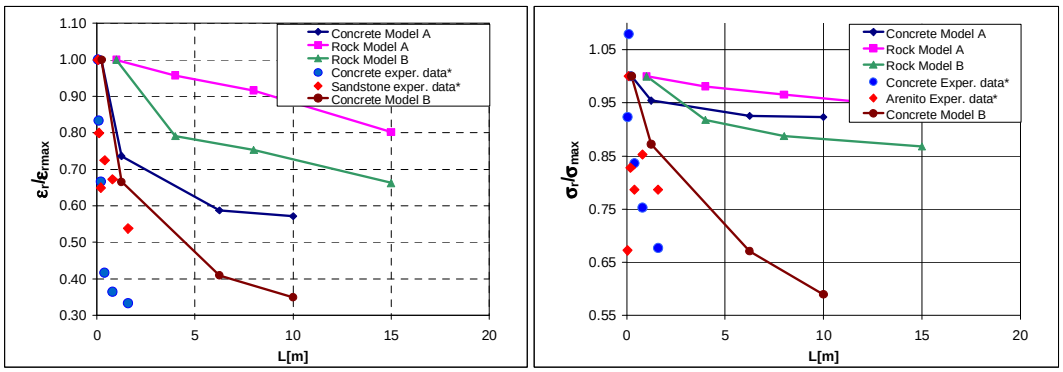

Figure 17 (a) Normalized rupture strain, (b) Normalized mean tensile strength, for various sizes estimated by simulation and obtained experimentally by Van Vliet and Van Mier [18], for concrete and rock plates.

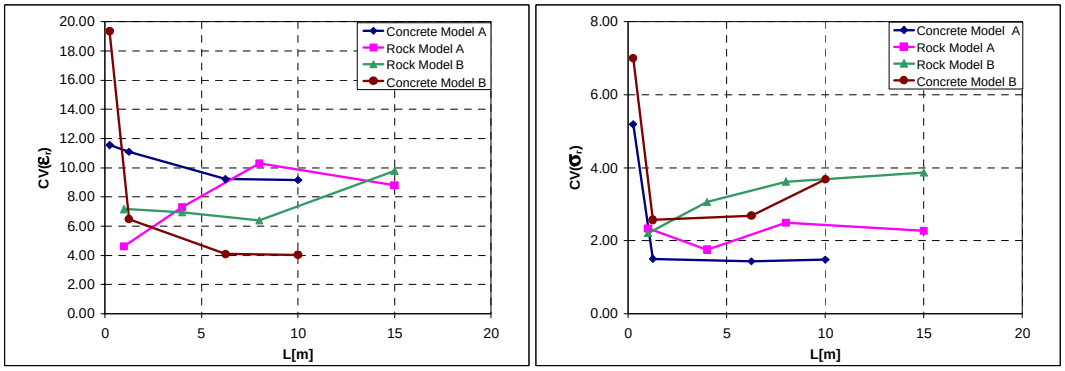

Figure 18 (a) Coefficients of variation of rupture strain, (b) Coefficients of variation of the tensile strength, estimated by simulation, for concrete and rock plates.

5 ON MESH DEPENDENCE IN DEM FRACTURE PREDICTIONS

The authors quantified size effects in the assessment of rupture of concrete or rock structures subjected to static or dynamic loading employing discrete elements of the same size (Rocha and Riera, [17]; Rios and Riera, [15]; Miguel *et al.*, [8]). In 3-D problems involving large systems, such as NPP containments, dams or rock foundations, larger elements must be resorted in order to reduce computational costs or to simply render the analysis feasible. Dalguer *et al.* [2] studied the formation of new cracks in rock layers during an earthquake employing DEM elements with a very large size (several hundred meters) and assumed for that purpose the constitutive relations for rock. Recognizing the need to reliably assess those relations, for which direct experimental evidence is definitely out of reach, Riera and Iturrioz [11] suggested the following scheme: determine the constitutive relations of large cubes by simulating tensile tests up to failure of 3-D models, employing constitutive elements of a size that can be tested in laboratory experiments. By repeating the scheme, the response of very large bodies could be theoretically inferred.

To illustrate the approach, the effective stress-strain curves shown in Figure 8 for plates with sizes ranging from 1.0 to 15.0m will be used. All of them were computed with models consisting of basic 0.1m elements, which are characterized by the stress-strain diagram shown in Figure 2, derived in turn from laboratory tests. Now, it is clear that 1m elements would present the stress-strain curve indicated in gray, while 15m elements would present the curve drawn in red (Figure 8). Use of larger elements requires re-evaluation of the properties of the random fields that define material properties, in this case *Gf*, subject discussed in detail by Riera and Iturrioz [11]. In this reference however, an important issue was not taken into consideration: the energy dissipated in the process of rupture is computed by means of Equation (3) which, if the coefficients *ca* indicated in Section 2 are used, implies that only one crack goes through the element. As clearly shown by Figures 11 and 12 and in uncountable laboratory experiments, in large plates or cubes the total fracture surface may largely exceed the minimum fracture surface needed to separate the plate or cube in two parts.

From the preceding reasoning, it is clear that when employing larger elements with length *L0*, care must be taken to preserve the energy dissipated in the rupture process, condition that may be satisfied by calculating a new fractured area *Af*, as follows: $A_f = c_a^* L_0^2$ (5)
in which the modified coefficient *ca** must be computed jointly with the evaluation of the effective stress-strain curves for the larger element and represents the ratio between the energy actually dissipated and the minimum energy required to split the element in two parts, given by Equation (3). One difficulty is that the energy depends on the stress field applied, which can be visually confirmed by inspecting Figures 11 and 12. The fractured areas for a given plate size are not the same.

Research is presently under way to develop criteria to predict values of *ca** for elements of various sizes, which is not an easy task because *ca** is not independent of the scale of correlation of material properties.

6 CONCLUSIONS

It was confirmed in this examination of the tensile fracture behavior of concrete and rock plates that predictions of fracture of non-homogeneous materials using DEM models are feasible and yield results that are consistent with the scarce experimental evidence so far available. The use of large elements, in which extensive cracking within the elements of the model may be expected, requires additional research, since the approach has proved successful only in cases where there is intense fracture localization, while tending to underestimate the strength otherwise.

Acknowledgements The authors acknowledge the support of CNPq and CAPES (Brazil).

References

[1] L. A. Dalguer, K. Irikura, J. D. Riera, and H. C. Chiu. The importance of the dynamic source effects on strong ground motion during the 1999 Chi-Chi, Taiwan, earthquake: Brief interpretation of the damage distribution on buildings. *Bull. Seismol. Soc. Am.*, 91:1112–1127, 2001.

[2] L. A. Dalguer, K. Irikura, and J. D. Riera. Simulation of tensile crack generation by three-dimensional dynamic shear rupture propagation during an earthquake. *J. Geophys. Res.*, 108(B3):2144, 2003.

[3] Y. Hayashi. Sobre uma representação discreta de meios contínuos em dinâmica não-linear. Master's thesis, CPGEC, Universidade Federal do Rio Grande do Sul, Porto Alegre, Brazil, 1982.

[4] I. Iturrioz. *Aplicação do método dos elementos discretos ao estudo de estruturas laminares de concreto armado*. PhD thesis, CPGEC, Universidade Federal do Rio Grande do Sul, Porto Alegre, Brazil, 1995.

[5] L. F. F. Miguel. *Critério constitutivo para o deslizamento com atrito ao longo da falha sísmica*. PhD thesis, PPGEC, Escola de Engenharia, Universidade Federal do Rio Grande do Sul, Porto Alegre, Brazil, 2005.

[6] L. F. F. Miguel and J. D. Riera. A constitutive criterion for the fault: modified velocity-weakening law. *Bull. Seismol. Soc. Am.*, 97(3):915–925, 2007. doi:10.1785/0120060107.

[7] L. F. F. Miguel, J. D. Riera, and L. A. Dalguer. Macro constitutive law for rupture dynamics derived from micro constitutive law measured in laboratory. *Geophys. Res. Lett.*, 33(L03302), 2006. doi:10.1029/2005GL024912.

[8] L. F. F. Miguel, J. D. Riera, and I. Iturrioz. Influence of size on the constitutive equations of concrete or rock dowels. *International Journal for Numerical and Analytical Methods in Geomechanics*, 32:1857–1881, 2008.

[9] A. H. Nayfeh and M. S. Hefzy. Continuum modeling of three-dimensional truss-like space structures. *AIAA Journal*, 16(8):779–787, 1978.

[10] J. D. Riera and I. Iturrioz. Discrete elements model for evaluating impact and impulsive response of reinforced concrete plates and shells subjected to impulsive loading. *Nuclear Engineering and Design*, 179:135–144, 1998.

[11] J. D. Riera and I. Iturrioz. On the fracture analysis of concrete structures taking into consideration size effects. In *SMiRT 18: International Conference on Structural Mechanics in Reactor Technology*, Beijing, China, 2005.

[12] J. D. Riera, L. F. F. Miguel, and L. A. Dalguer. On the constitutive criteria for the fault: Influence of size and tensile cracks generation during rupture. In *SMiRT 18: International Conference on Structural Mechanics in Reactor Technology*, Beijing, China, 2005.

[13] J. D. Riera, I. Iturrioz, and L. F. F. Miguel. On mesh independence in dynamic fracture analysis by means of the discrete element method. In *ENIEF 2008: XVII Congreso sobre Métodos Numéricos y sus Aplicaciones, Mecanica Computacional*, volume XXVII, pages 2085–2097, San Luis, Argentina, 2008.

[14] R. D. Rios. *Aplicações do método dos elementos discretos em estruturas de concreto*. PhD thesis, PPGEC, Universidade Federal do Rio Grande do Sul, Porto Alegre, Brazil, 2002.

[15] R. D. Rios and J. D. Riera. Size effects in the analysis of reinforced concrete structures. *Engineering Structures*, 26: 1115–1125, 2004.

[16] M. M. Rocha. Ruptura e efeitos de escala em materiais não-homogêneos. Master's thesis, CPGEC, Universidade Federal do Rio Grande do Sul, Porto Alegre, Brazil, 1989.

[17] M. M. Rocha and J. D. Riera. On size effects and rupture of nonhomogeneous material. In J. G. M. Van Mier, J. G. Rots, and A. Baker, editors, *Congress in Fracture Processes in Concrete, Rock and Ceramics*, pages 451–60, London, 1990. Chapmen & Hall/Ed. Fn. Spon.

[18] M. R. A. Van Vliet and J. G. M. Van Mier. Size effect of concrete and sandstone. *Heron*, 45(2):91–108, 2000.